

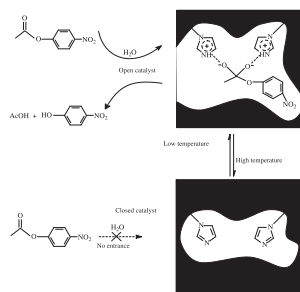


Contents

'On/off'-switchable catalysis by a smart enzyme-like imprinted polymer

pp 173–180

Songjun Li*, Yi Ge*, Ashutosh Tiwari, Shenqi Wang, Anthony P.F. Turner, Sergey A. Piletsky

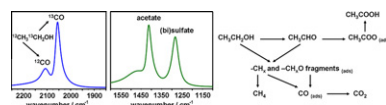


By creating a thermosensitive hydrophilic/hydrophobic transition within the imprinted networks, the prepared enzyme-like imprinted catalyst was capable of 'yes/no'-regulated access to the reactants, leading to 'on/off'-switchable catalysis.

Reaction pathways of ethanol electrooxidation on polycrystalline platinum catalysts in acidic electrolytes

pp 181–188

Robert B. Kutz, Björn Braunschweig, Prabhuddha Mukherjee, Rachel L. Behrens, Dana D. Dlott, Andrzej Wieckowski*

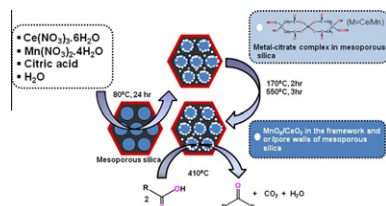


Potentiodynamic broadband sum-frequency generation and electrochemistry were used to elucidate the mechanism of ethanol electrooxidation on polycrystalline platinum in acidic electrolytes.

Supported mesoporous solid base catalysts for condensation of carboxylic acids

pp 189–199

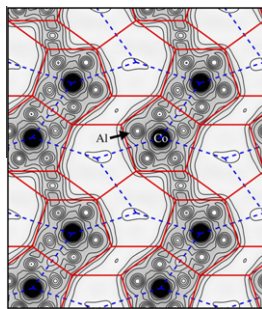
Ambareesh D. Murkute, James E. Jackson, Dennis J. Miller*



New mesoporous solid base catalysts, abbreviated as CM-HMS and CM-MCM-41, were synthesized by incorporating active base centers of MnO_x/CeO_2 into two different mesoporous silica supports (HMS and MCM-41). CM-HMS and CM-MCM-41 are more efficient catalysts than unsupported MnO_x/CeO_2 in ketonization of carboxylic acids.

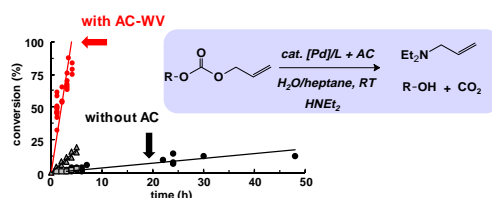
Complex intermetallic compounds as selective hydrogenation catalysts – A case study for the (100) surface of $\text{Al}_{13}\text{Co}_4$ pp 200–207

Marian Krajičí, Jürgen Hafner*

Electron density distribution in the catalytically active (100) surface of $\text{Al}_{13}\text{Co}_4$.**Scope and limitation of activated carbons in aqueous organometallic catalysis**

pp 208–218

Nicolas Kania, Narasimhan Gokulakrishnan, Bastien Léger, Sophie Fourmentin, Eric Monflier, Anne Ponchel*

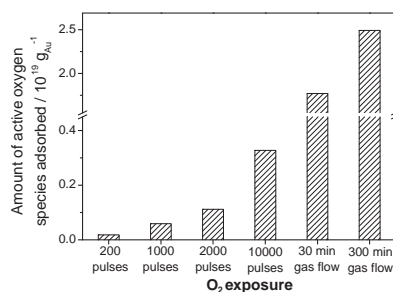


Addition of activated carbon, with appropriate physicochemical characteristics, appears as a simple and efficient method to solve mass-transfer limitations in aqueous organometallic catalysis. New insights into the role of carbon support during the catalytic course are reported.

Dynamic studies of CO oxidation on nanoporous Au using a TAP reactor

pp 219–227

L.C. Wang, H.J. Jin, D. Widmann, J. Weissmüller, R.J. Behm*

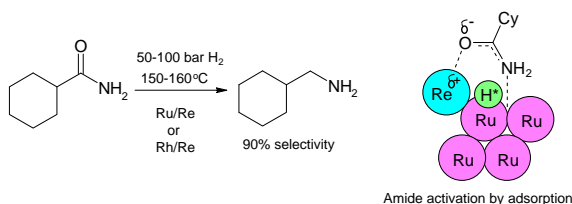


The oxidation of CO on nanoporous Au, in particular the activation of molecular O_2 , was investigated by a combination of kinetic and TAP measurements, showing the formation of stable adsorbed active oxygen via dissociative O_2 adsorption.

Selective hydrogenation of amides using bimetallic Ru/Re and Rh/Re catalysts

pp 228–238

Graham Beamson, Adam J. Papworth, Charles Philipps, Andrew M. Smith, Robin Whyman*

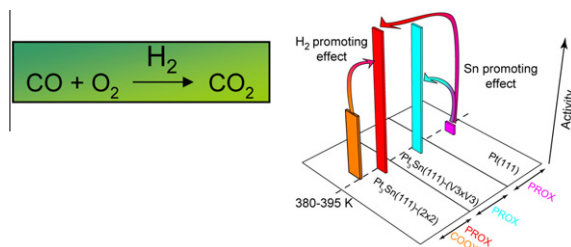


Recyclable Ru/Re and Rh/Re bimetallic catalysts are effective for the highly selective (90%) reduction of primary amides such as CyCONH_2 to the corresponding primary amine CyCH_2NH_2 .

Preferential CO oxidation in a large excess of hydrogen on Pt₃Sn surfaces

pp 239–245

C. Dupont, F. Delbecq, D. Loffreda, Y. Jugnet*

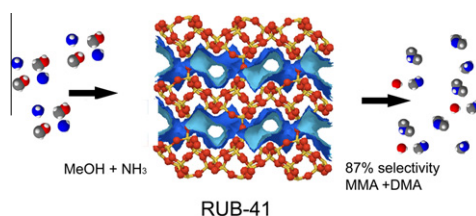


Both Sn and H₂ promote CO oxidation on Pt₃Sn(1 1 1) surfaces. The surface structure sensitivity in CO oxidation is cancelled out when the reaction is performed under a large excess of hydrogen.

Shape-selective synthesis of methylamines over the RRO zeolite Al-RUB-41

pp 246–252

Bart Tijsebaert, Bilge Yilmaz, Ulrich Müller, Hermann Gies, Weiping Zhang, Xinhe Bao, Feng-Shou Xiao, Takashi Tatsumi, Dirk De Vos*



Shape-selective amination of methanol over Al-RUB-41 with selectivities up to 87% towards monomethylamine and dimethylamine.

Thiotolerant Ir/SiO₂-Al₂O₃ bifunctional catalysts: Effect of metal–acid site balance on tetralin hydroconversion

pp 253–265

Salim Nassreddine, Laurence Massin, Mimoun Aouine, Christophe Geantet, Laurent Piccolo*

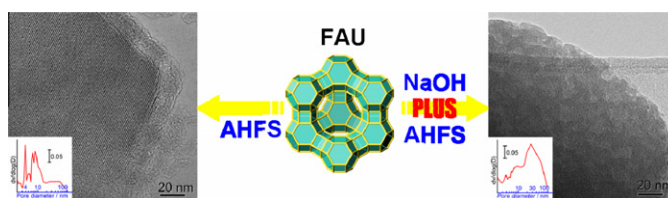


Ir supported on amorphous silica–alumina is sulfur tolerant and catalyzes tetralin hydrogenation, ring contraction, and ring opening without cracking. The selectivity to ring opening increases with the acid/metal site ratio.

Mesoporous Y zeolite with homogeneous aluminum distribution obtained by sequential desilication–dealumination and its performance in the catalytic cracking of cumene and 1,3,5-triisopropylbenzene

pp 266–275

Zhengxing Qin, Baojian Shen*, Xionghou Gao, Feng Lin, Baojie Wang, Chunming Xu

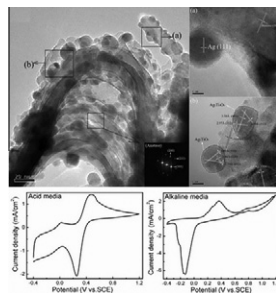


AHFS dealumination leads to severe non-uniform dealumination of zeolite framework and substantial surface silicon deposition. Sequential desilication and dealumination affords sample with mesopore formation and noteworthy improved aluminum–silicon distribution.

Silver nanoparticles supported on TiO₂ nanotubes as active catalysts for ethanol oxidation

pp 276–287

Y.Q. Liang, Z.D. Cui, S.L. Zhu, Y. Liu, X.J. Yang*

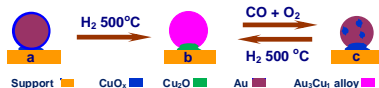


The TEM micrographs for Ag doped TiO₂ nanotubes annealed at 723 K and the cyclic voltammograms in acidic and alkaline media.

Structural changes of Au–Cu bimetallic catalysts in CO oxidation: In situ XRD, EPR, XANES, and FT-IR characterizations

pp 288–296

Xiaoyan Liu, Ai Qin Wang, Lin Li, Tao Zhang*, Chung-Yuan Mou*, Jyh-Fu Lee

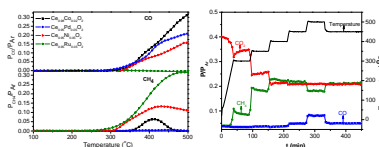


The structural changes of SBA-15-supported Au–Cu bimetallic nanoparticles were studied by in situ techniques. The freshly reduced catalyst is mainly composed of Au₃Cu₁ alloy, which was segregated into a gold core decorated with patches of CuO_x on the surface during the reaction of CO oxidation.

CO₂ methanation on Ru-doped ceria

pp 297–309

Sudhanshu Sharma, Zhenpeng Hu, Peng Zhang, Eric W. McFarland, Horia Metiu*

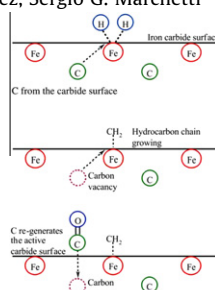


The performance of doped ceria for CO₂ reaction with CH₄.

Effect of the activation atmosphere on the activity of Fe catalysts supported on SBA-15 in the Fischer–Tropsch Synthesis

pp 310–320

Leonardo A. Cano, María V. Cagnoli, José F. Bengoa, Ana M. Alvarez, Sergio G. Marchetti*

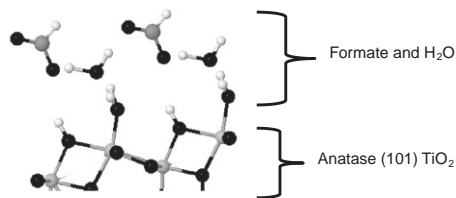


Fischer-Tropsch synthesis on Fe/SBA-15 supported catalysts was studied to probe the effect of the activation atmosphere on the structural properties. Higher production of total hydrocarbons, higher CO conversion and higher selectivity towards light olefins are obtained when the catalyst is activated in H₂. These results are explained considering that the iron carbides produced from α -Fe are more active than that obtained from Fe₂O₃.

Effect of water on the adsorbed structure of formic acid on TiO₂ anatase (1 0 1)

pp 321–328

Kristi L. Miller, John L. Falconer, J. Will Medlin*

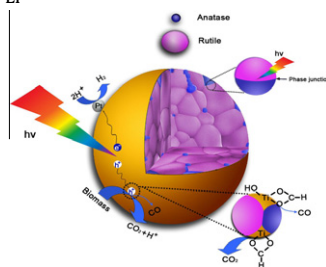


Density functional theory calculations showed water co-adsorbed with formic acid promoted O–H bond dissociation on anatase (1 0 1) depending on formic acid and water coverage. The addition of water also stabilized monodentate formate relative to bidentate formate.

Enhancing hydrogen production activity and suppressing CO formation from photocatalytic biomass reforming on Pt/TiO₂ by optimizing anatase–rutile phase structure

pp 329–335

Qian Xu, Yi Ma, Jing Zhang, Xiuli Wang, Zhaochi Feng, Can Li*



For photocatalytic biomass reforming on Pt/TiO₂ by tuning anatase–rutile phase structure, the hydrogen production activity can be significantly enhanced and CO concentration can be reduced from thousands ppm to 5 ppm.